Probing elastic properties of graphene and heat conduction in graphene bubbles above 1000 °C

Wolfgang Bacsa [*]
CEMES-CNRS and Université de Toulouse, Toulouse 31055, France

Frédéric Topin
Aix Marseille Univ, CNRS, IUSTI, Marseille 13001, France
and LAPLACE CNRS, University of Toulouse, Toulouse 31055, France

Marc Miscevic
LAPLACE, UMR CNRS-INP-UPS 5213, University of Toulouse, Toulouse 31055, France

James M. Hill
University of South Australia, Adelaide, South Australia 5001, Australia

Yuan Huang
Advanced Research Institute of Multidisciplinary Science, Beijing Institute of Technology, Beijing 100081, China

Rodney S. Ruoff
Center for Multidimensional Carbon Materials (CMCM), Institute for Basic Science (IBS), Ulsan 44919, Republic of Korea;
Department of Chemistry, Ulsan National Institute of Science and Technology (UNIST), Ulsan 44919, Republic of Korea;
Department of Materials Science and Engineering, Ulsan National Institute of Science and Technology (UNIST),
Ulsan 44919, Republic of Korea;
and School of Energy and Chemical Engineering, Ulsan National Institute of Science and Technology (UNIST),
Ulsan 44919, Republic of Korea

The elastic and thermal properties of graphene were investigated by illuminating graphen bubbles with a laser spot. Tempertures above 1000 °C were obtained in large (>10 μm) graphene bubbles. The formation of standing optical waves lead to laser heating depending on the height of the garphene bubble, which results in Raman band oscillations when scanning the laser spot across the bubble. The profile of the bubble under laser illumination can be deduced from the Raman G band oscillations. A distinct swelling at the center of the bubble is observed which is attributed to the strong softening of graphene above 1000 °C. From the size and height of the swelling it is deduced that the elastic modulus is reduced by at least 40% at 1000 °C. On solving the heat equation for the heat dissipation through the graphene only, analytical expressions are obtained for the isotherms on the bubble for both symmetrical and asymmetrical positions of the laser spot. It was found that a large fraction of the absorbed heat dissipates through the gas in the bubble using the finite volume method. Analytical expressions for the temperature distribution in the bubble are deduced from the numerical results. Heat conduction through the gas in the bubble influences the temperature distribution and needs to be taken into account in the heat dissipation in graphene bubbles.

I. INTRODUCTION

Graphene has superior mechanical properties. The breaking force obtained experimentally and from simulation are almost identical and the experimental value of the second-order elastic stiffness is equal to $E_{2D} = 340 \pm 50$ Nm^{-1}. This value corresponds to a Young's modulus of $E = 1.0 \pm 0.1$ TPa, assuming an effective thickness of 0.335 nm [1]. The ultimate tensile strength of 119 GPa at room temperature was reported to have a high temperature stability [2]. Joule heating in transmission electron microscopy (TEM) reportedly showed that suspended graphene stays intact up to temperatures of 1275 K and it was estimated that graphene stays stable up to temperatures of 2600 K [3]. However, only a few theoretical studies are available on the elastic modulus of graphene up to 1000 K [2] and there are no reported experimental studies so far on the elastic properties of graphene at elevated temperatures. It is reported that the presence of ripples and interaction with the substrate can notably affect the mechanical response of graphene [4], and it is therefore important to study suspended graphene. In this context, graphene bubbles can be effectively used since they can be heated with a laser beam and since graphene is detached from the substrate in the bubble, substrate interactions are avoided. Thus, heating graphene bubbles by a laser beam provides a unique opportunity to

*wolfgang.bacsa@cemes.fr

explore the thermal and the elastic properties of graphene since the bubble height to diameter ratio is directly related to the Young's modulus. The temperature at the laser spot on the graphene bubble can be deduced from Raman spectral band shifts. Since the laser intensity is not uniform in a direction perpendicular to the substrate due to the formation of standing waves, the Raman shift oscillates when scanning the laser spot across the bubble (4). From the period of the standing wave, the height of the bubble at the laser spot can be determined. The temperature distribution in graphene bubbles heated with a laser beam is reported to have a logarithmic dependence on bubble radius [5] and the highest temperature which can be reached at the center of the bubble increases with bubble size for a given laser power. This means in large graphene bubbles, very high temperatures can be reached, in contrast to simply heating graphene below 1000 °C, which leads to only small changes in the lattice constant since the contributions of the transverse and in-plane phonon population with temperature have opposite effects [6] on the lattice constant and this is manifest at "lower" temperature. For example, the thermal expansion coefficient (TEC) is slightly negative below 430 K and is slightly positive above 430 K (4.2710–6/K@1000 K), and the Debye temperature, which is a measure of the hardness and heat capacity, for graphene (2100 K) [7] is higher than in most solids except diamond (2200 K). With an increase in temperature, one theory study suggested that from 0 K to 1000 K, c_{11} softens by 2.51% and Young's modulus E decreases by 2.2%, and the ultimate strength decreases by 4.03% from 0 K to 1000 °C [2].

In our previous work on Raman spectroscopy of graphene bubbles, we showed that large graphene bubbles (12 μm) can be heated to above 1000 °C when illuminated with a laser beam [5] leading to the formation of standing waves. This means that laser heating of the bubble depends upon the bubble height at the location of the laser spot assuming the graphene does not influence the standing wave. Depending upon the position of the standing wave with respect to the graphene and the location on the bubble, oscillations of the Raman peak position can be observed when scanning across the graphene bubble. The spectral position of the phonon peak depends on temperature [5] and from the Raman oscillation one can extract the temperature of the graphene bubble for a given laser power at a particular location as well as the contour of the bubble. The highest so-deduced temperature was above 1000 °C.

Here, we revisited the Raman spectral data of graphene bubbles since a closer examination of the Raman oscillactions indicated smaller oscillations at the center of the bubble. Our spectral analysis shows a clear "swelling" at the center of the bubble where the temperature is highest, and the temperature at the edge of the swelling is found to be close to 1000 °C. Above 1000 °C, this swelling of the bubble indicates that the graphene has softened so that there is a reduction in the Young's modulus. In the following, we take into account the heat dissipation through the gas inside the bubble, and we provide an analytical model calculation of the heat conduction though the bubble wall for both symmetric and asymmetric illumination. These model calculations indicate that heat conduction though the gas inside the bubble is significant and only a part of the heat flows though the bubble wall.
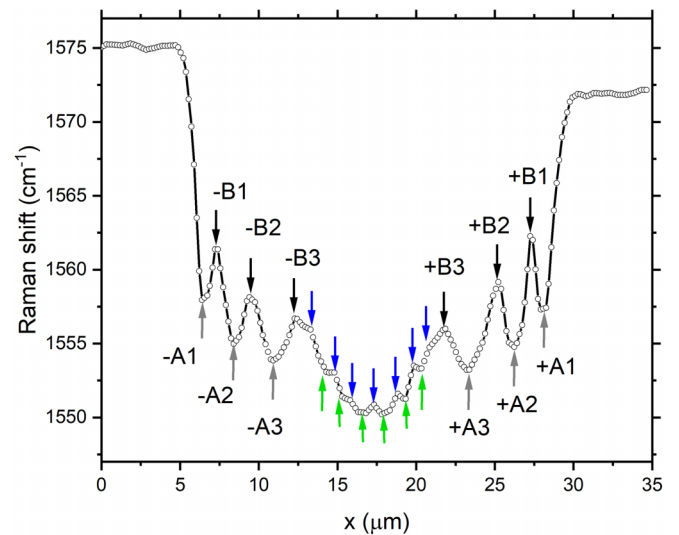

FIG. 1. Raman G band across graphene bubble. Main oscillations due to optical standing wave are labeled and numbered (A: minima, B: maxima). The smaller oscillations in the center portion are shown with green and blue arrows.

II. EXPERIMENTAL RESULTS

Figure 1 shows the spectral position of the Raman G band when scanning the laser spot (532 nm, 20 mW) across the bubble. The graphene bubble was created by placing graphene on a hot SiO_2 (100 nm)/Si substrate; details of the preparation and characterization are given in our previous publication [5]. Since the incident beam is reflected off the substrate, the two beams interfere to form an optical standing surface wave and its first maximum falls on the SiO_2 surface of the substrate [8]. The Raman G band shifts when the graphene is heated and oscillations in Raman spectral shifts are observed when scanning the laser beam across the bubble since the distance between the graphene and the substrate changes across the bubble. It is known that, in addition to temperature, spectral shift in the Raman G band is also influenced by strain and doping [9]. The doping-induced shift can be estimated by the differences observed of the G band position at 0 and 35 μm (2.6 cm^{-1}) in Fig. 1, while the strain can be deduced by the ratio of the circular arc to the bubble diameter (0.5%), which results in a strain-induced downshift of 10 cm^{-1} [10]. Taking strain- and doping-induced reductions into account, the remaining spectral shifts are then attributed to temperature variations caused by the optical standing waves. The oscillations in the temperature primarily arise from the location of the maxima and minima of this standing wave. As the spacing between the interference fringes in the standing wave perpendicular to the substrate is half the wavelength, it is possible to deduce the shape of the bubble under laser radiation from the Raman spectral oscillations, and Fig. 2 shows the so-determined shape of the bubble. In Fig. 1, a second minimum is observed next to $+B3$, $-B3$ which are assumed to be at the same height. When calculating the field near the SiO_2 (100 nm)/Si substrate, the optical standing wave near the substrate has a local intensity which varies between 0.43 and 1.85 times the intensity in the incident beam [8]. The smaller amplitudes of the oscillations at the center are
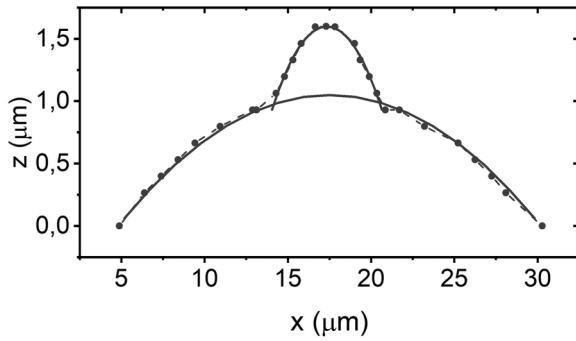
FIG. 2. The position of graphene above the substrate at the laser spot is deduced from the Raman spectral oscillations in Fig. 1. The bubble is higher at the center ("swelling") due to the higher temperature; the thermal resistance is highest at the center of the bubble. The shape obtained from the graphene height (obtained at the laser spot when scanning across the bubble), can be approximated by a spherical shape: one for the bubble and one for the swelling ($h_1 = 1.05$ μm, $r_1 = 12.7$ μm, $h_2 = 0.9$ μm, $r_2 = 3.8$ μm). The vertical scale is enlarged to make the swelling region apparent.

attributed to the fact that the oscillations are closer spaced and smaller than the size of the focal spot as compared to the oscillations at the edge of the bubble.

The extracted profile in Fig. 2 shows that instead of a flat top, the bubble has a pronounced swelling which is 7 μm in size and 0.6 μm high. Graphene is heated at the laser spot and the temperature increase is higher in the center region where the swelling occurs due to its larger thermal resistance. It is assumed that the shape when illuminated at the center of the bubble is similar to the shape observed in Fig. 2. The swelling is smaller when the laser spot is slightly off center, and it is assumed that the shape will be similar but asymmetric. It is important to bear in mind that the bubble shape under illumination is not directly measured and that the profile shown in Fig. 2 corresponds to the height of the bubble when illuminated at a particular location on the bubble. The bubble's increased height at the center indicates that the elastic constants and thus bending rigidity are reduced there. The volume change is small because the pressure change is small inside the bubble. The profile of this central region is most likely similar to that shown in Fig. 2 when the laser spot hits the bubble at the center. The higher curvature in the "swelling region" means that the graphene elastic constant is significantly reduced "in the swelling region" where the temperature reaches more than 1000 °C. Clearly the size of the swelling coincides with the region with temperatures higher than 1000 °C (Fig. 3). The solid line in Fig. 2 shows a hemispherical bubble shape which is adjusted to the bubble cross section (radius 12 μm, height 1 μm). While the shape of the bubble is not exactly spherical due to its constraints from the edge, deviations from a spherical shape were not observed and are considered to be small [5]. We note that the x and y axes are not at the same scale and hence the spherical shape of the bubble is not apparent. The larger curvature in the "swelling region" (radius: 3.5 μm, height $h = 0.6$ μm) implies a larger strain (2%) calculated from radius and height. Adopting this strain-induced reduction for the Raman band frequency of graphene this would imply a down shift of 40 cm^{-1} which
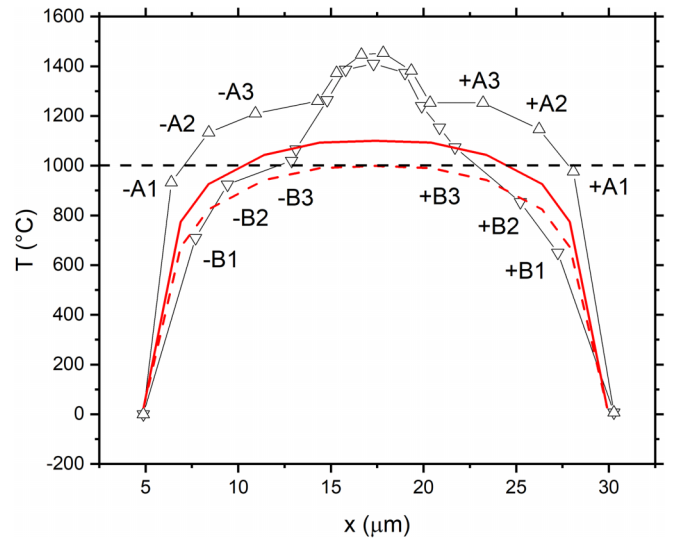

FIG. 3. Deduced temperature across the bubble from points A and B in Fig. 1. The bubble temperature is above 1000 °C everywhere other than the edge. The temperature in the central region of the bubble is higher but not well determined. The red curve shows the temperature deduced from finite element analysis (Sec. III C). The maximum temperature (full line) and mean temperature (dashed line) across the bubble profile are shown.

is larger than the total reduction 29 cm^{-1}. This indicates either that the reduction of the elastic modulus in the swelling reduces the strain-induced down shift of the Raman G band or the graphene expansion is significantly larger at 1000 °C. As a result, the deduced temperature for the swelling is not accurate since the temperature-induced shift depends on the elastic constants.

From the radius and height of the bubble and also of the swelling region the volume and the surface of each can be calculated yielding 208 μm^3 and 6 μm^3 and 418 μm^2 and 24.5 μm^2, respectively. The volume of the swelling corresponds to 2.9% of the bubble volume and 5.9% of the bubble surface. The surface of this "spherical cap" ("swelling region") can be compared with the surface without this local curvature due to local swelling, which gives an 0.8% increase for the bubble (whole bubble) and 3.3% increase for the swelling due to the large curvature.

Figure 3 shows the deduced temperature across the bubble for the minima and maxima. Using the reported temperature-induced shift of the G band 0.015 cm^{-1}K^{-1} [11], we may deduce that the temperature reaches 1000 °C at B3. In Fig. 1 three large oscillations are seen in the outer region (labeled with A and B) and smaller oscillations are seen in the central region (arrows). The temperature in the center of the region cannot be deduced by the Raman shift since the strain-induced shift is modified due to the smaller elastic constants and is not known as such, however, the temperature at the edge can be deduced.

III. THERMAL TRANSPORT

In our earlier work, analytical expressions were derived for the temperature distribution when the bubble is illuminated

at its center and the temperature distribution for of-center illumination was obtained numerically [5]. Here, we show that analytical expressions can be obtained also for off-axis illumination. For completeness, the derivation of the expression for on-axis illumination is included. As a first step we consider only heat conduction within the graphene layer of the bubble with a fixed temperature at the edge. As the bubble height is considerably smaller than the diameter, the bubble is represented by a flat disk of radius r_2 which is illuminated through a circular spot with radius r_1. Since heat loss through radiation is less than a couple of percent and through convection is less than 0.2% they are both neglected. Further heat loss through the fluid in the bubble is at first neglected (Sec. III A) and then considered in detail in Sec. III B.

A. Heat conduction through graphene only

The effect of the laser spot on graphene is considered by placing the laser beam at the center of the bubble and assuming that the graphene is a thermally thin layer of thickness z. The heat equation for steady-state and constant thermal conductivity k is then, using cylindrical symmetry

$$\frac{d}{dr}\left(r\frac{dT}{dr}\right) = 0, \tag{1}$$

and integration yields $T(r) = A_1 \ln(r) + A_2$, where A_1 and A_2 are constants that can be determined by considering the two following boundary conditions:

$$Q = -k2\pi r_1 z \left(\frac{dT}{dr}\right)_{r=r_1}, \tag{2}$$

$$T(r_2) = T_2. \tag{3}$$

The constants A_1 and A_2 can then be eliminated to give

$$T(r) = \frac{-Q}{2\pi kz} \cdot \ln\left(\frac{r}{r_2}\right) + T_2. \tag{4}$$

In terms of thermal resistance (R_{th}) for $r_1 < r < r_2$ the temperature distribution is:

$$T(r) = Q \cdot R_{\text{th}}(r) + T_2, \tag{5}$$

where the thermal resistance $R_{\text{th}}(r)$ between r and r_2 is defined by

$$R_{\text{th}}(r) = \frac{-\ln(r/r_2)}{2\pi kz}, \tag{6}$$

when placing the laser spot on the bubble but off center, the temperature distribution is no longer one dimensional. However, a coordinate transformation can be used to obtain again a one-dimensional temperature distribution following Carslaw and Jaeger [12]. This transformation uses the fact that if ξ and η are conjugate functions of x and y defined so that $\xi + i\eta = f(x + iy)$. The temperature distribution T satisfies the Laplace equation in the $\xi\eta$-plane if it satisfies it in the xy-plane. For two nonconcentric circles, the following conjugate functions ξ and η of x and y are considered:

$$\xi = \ln\left(\frac{BM}{AM}\right), \tag{7}$$

$$\eta = \beta_1 - \beta_2, \tag{8}$$

where A and B are two points in the xy-plane at coordinates $(\delta; 0)$ and $(-\delta; 0)$, respectively, and M is the point where the temperature needs to be determined at coordinates $(x; y)$. β_1 and β_2 are the angles $\angle(\overrightarrow{Ox}; \overrightarrow{AM})$ and $\angle(\overrightarrow{Ox}; \overrightarrow{BM})$ made by AM and BM with the x axis (in the positive direction). With this transformation, the xy-plane is given by $-\pi < \eta < \pi$ and $-\infty < \xi < +\infty$. ξ is expressed as a function of x and y:

$$\xi = \frac{1}{2} \ln\left(\frac{(x+\delta)^2 + y^2}{(x-\delta)^2 + y^2}\right). \tag{9}$$

For two nonconcentric circles in the xy-plane located at C_1 and C_2 on the x-axis (i.e., $\eta = 0$) and separated by the distant ℓ, this transformation makes the problem one dimensional in the $\xi\eta$-plane. The larger circle is defined by ξ_2, while the smaller circle is defined by ξ_1 and two diametrically opposite points of a circle have the same coordinate ξ. If for circle 1

$$\xi_1 = \ln\left(\frac{x_{C_1} + r_1 + \delta}{x_{C_1} + r_1 - \delta}\right) = \ln\left(\frac{x_{C_1} - r_1 + \delta}{x_{C_1} - r_1 - \delta}\right). \tag{10}$$

It can be deduced that

$$\delta^2 = x_{C_1}^2 - r_1^2, \tag{11}$$

the same is valid for circle 2

$$\delta^2 = x_{C_2}^2 - r_2^2. \tag{12}$$

Using $\ell = x_{C_2} - x_{C_1}$, it follows that

$$x_{C_1} = (r_2^2 - r_1^2 - \ell^2)/2\ell, \tag{13}$$

and

$$x_{C_2} = (r_2^2 - r_1^2 + \ell^2)/2\ell, \tag{14}$$

and δ can be deduced from the coordinates of locations of the center of the two circles

$$\delta = \sqrt{\left(\frac{r_2^2 - r_1^2 - \ell^2}{2\ell}\right)^2 - r_1^2} = \sqrt{\left(\frac{r_2^2 - r_1^2 + \ell^2}{2\ell}\right)^2 - r_2^2}. \tag{15}$$

It follows that

$$\xi_1 = \ln\left(\frac{x_{C_1} + \sqrt{x_{C_1}^2 - r_1^2}}{r_1}\right) = \text{arcosh}\left(\frac{x_{C_1}}{r_1}\right), \tag{16}$$

$$\xi_2 = \ln\left(\frac{x_{C_2} + \sqrt{x_{C_2}^2 - r_2^2}}{r_2}\right) = \text{arcosh}\left(\frac{x_{C_2}}{r_2}\right). \tag{17}$$

In the $\xi\eta$-plane the temperature field is the solution of the one-dimensional Laplace equation

$$\frac{\partial^2 T}{\partial \xi^2} = 0, \tag{18}$$

and since the temperatures T_1 and T_2 are constant on the two circles $\xi = \xi_1$ and $\xi = \xi_2$, the solution depends only on ξ and is

$$T = T_1 \frac{\xi - \xi_2}{\xi_1 - \xi_2} + T_2 \frac{\xi_1 - \xi}{\xi_1 - \xi_2}. \tag{19}$$

Knowing the one-dimensional temperature field in the $\xi\eta$-plane, and integrating the Fourier law on the circle 1, the

absorbed heat power Q can be expressed as a function of ξ_1 and ξ_2:

$$Q = -2k\pi r_1 z \left(\frac{dT}{d\xi}\right)_{\xi=\xi_1} = -2\pi kz \frac{T_1 - T_2}{\xi_1 - \xi_2}. \quad (20)$$

The thermal resistance between the two circles is

$$R_{th} = \frac{T_1 - T_2}{Q} = \frac{\xi_1 - \xi_2}{2\pi kz}. \quad (21)$$

Using the relation

$$\operatorname{arcosh}(u) - \operatorname{arcosh}(v) = \operatorname{arcosh}(uv - \sqrt{(u^2 - 1)(v^2 - 1)}), \quad (22)$$

and the expression of the thermal resistance in the case of off-center illumination is finally

$$R_{th} = \frac{1}{2\pi kz} \operatorname{arcosh}\left(\frac{r_1^2 + r_2^2 - \ell^2}{2r_1 r_2}\right) \quad (23)$$

and the temperature at the periphery of the laser spot is

$$T_1 = Q \cdot R_{th} + T_2. \quad (24)$$

The isotherms T are then, in the Cartesian $\xi\eta$-plane, an iso-ξ of coordinate

$$\xi = \xi_2 - (\xi_2 - \xi_1)(T - T_2)/R_{th}Q. \quad (25)$$

In the case of off-center illumination, the isotherms are displaced circles whose location of the center $x_C(T)$ and radius $r(T)$ are (Fig. 4) given by

$$x_C(T) = -\frac{\delta \cosh \xi}{1 + \cosh \xi} \frac{1 + e^\xi}{1 - e^\xi} = \delta \frac{e^{2\xi} + 1}{e^{2\xi} - 1}, \quad (26)$$

$$r(T) = -\frac{\delta}{1 + \cosh \xi} \frac{1 + e^\xi}{1 - e^\xi} = \delta \frac{2e^\xi}{e^{2\xi} - 1}. \quad (27)$$

While the amount of laser power absorbed by the bilayer graphene is 4.6%, the laser power at a particular distance from the substrate varies due to the formation of optical standing wave. Taking into account the index of refraction of Si and SiO$_2$ the power at a maximum of the optical standing is 1.8 times the power of the incident field for Si/SiO$_2$ substrate. Note that this is not in contradiction with energy conservation because when averaged over the optical standing wave only 0.9 times of the laser power is available. That means $0.046 \times 1.8 = 0.083$ of the laser power is absorbed in the graphene in the standing wave maxima.

B. Symmetric heat conduction through graphene including gas in bubble

Graphene exchanges heat with its environment either through convection with air and radiation. The air inside the bubble, however, is confined preventing any convection to occur. Applying the energy balance between two circles of radius r and radius $r + dr$ at the center of the bubble in the radial and perpendicular direction

$$2\pi kz \frac{d}{dr}\left(r \frac{dT}{dr}\right) - 2\pi hr(T - T_{env}) = 0, \quad (28)$$

along with the boundary conditions described by Eqs. (2) and (3). Using $\theta = T - T_{env}$ the energy balance can be
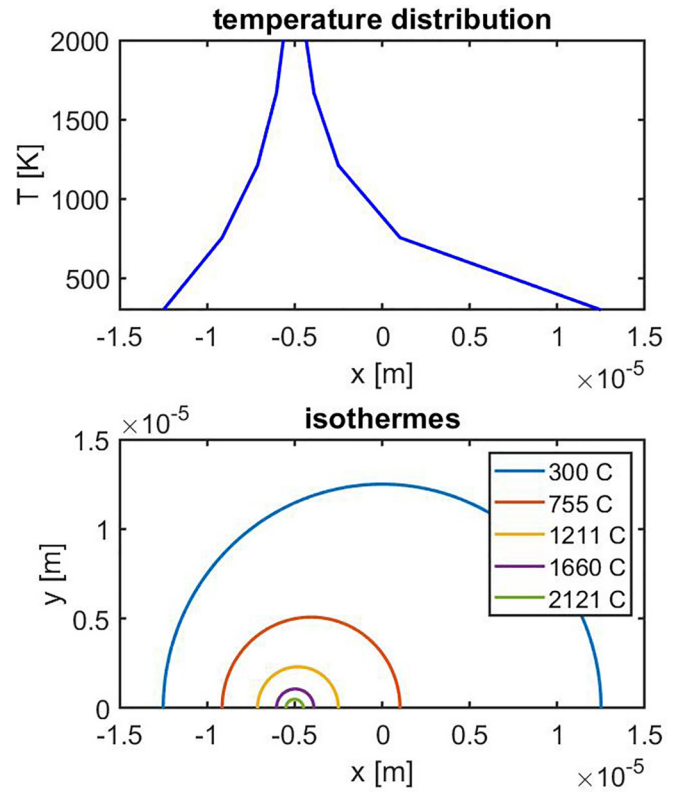

FIG. 4. Temperature distribution and isotherms on bubble when illuminated with laser spot in off-axis position. Temperature exceeds 2000 °C near laser spot.

rewritten as

$$\frac{d^2\theta}{dr^2} + \frac{1}{r}\frac{d\theta}{dr} - \frac{h}{kz}\theta = 0. \quad (29)$$

This later equation is a zero-order Bessel differential equation with the solution

$$\theta(r) = T(r) - T_{env} = k_1 J_0(i\beta r) + k_2 Y_0(-i\beta r), \quad (30)$$

where J_0 and Y_0 are Bessel functions of the first kind and second kind, respectively, and with

$$\beta = (h/zk)^{-1/2}.$$

The constants B_1 and B_2 can be expressed using the boundary conditions

$$B_1 J_0(i\beta r_2) + B_2 Y_0(-i\beta r_2) = \theta_2, \quad (31)$$

$$iB_2\beta Y_1(-i\beta r_1) - iB_1\beta J_1(i\beta r_1) = \frac{Q}{2\pi zkr_1}, \quad (32)$$

and expressions for B_1 and B_2 are then

$$B_1 = [2\pi zkr_1\beta\theta_2 Y_1(-i\beta r_1) - iQY_0(-i\beta r_2)]/D, \quad (33)$$

$$B_2 = [-2\pi zkr_1\beta\theta_2 J_1(i\beta r_1) + iQJ_0(i\beta r_2)]/D, \quad (34)$$

with

$$D = 2\pi zkr_1\beta[J_1(i\beta r_1)Y_0(-i\beta r_2) + J_0(i\beta r_2)Y_1(-i\beta r_1)].$$

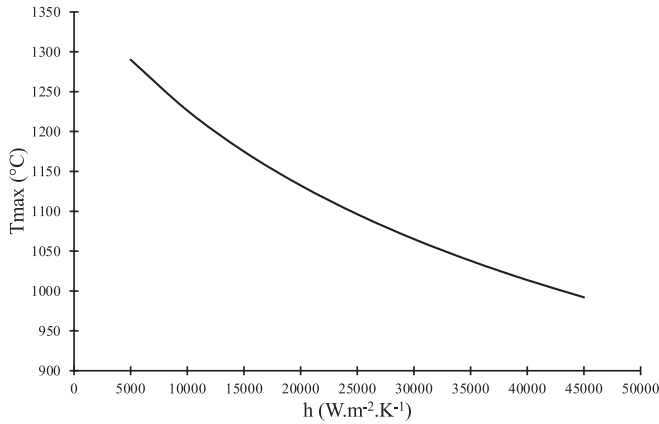FIG. 5. Temperature at center of graphene sheet as function of heat transfer coefficient h.
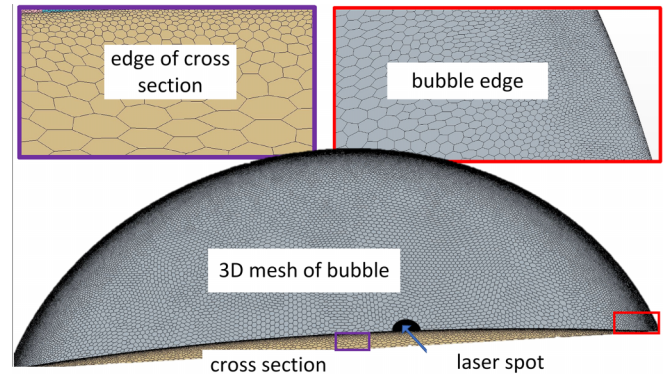

FIG. 6. Mesh structure (grey) in bubble wall and in vertical plane (yellow) across bubble. Laser spot shown in (blue). Rectangle on top, left side shows variation of mesh size in vertical plane. Rectangle on top, right side shows variation of mesh in bubble wall near border.

When including heat loss caused by convection and radiation the heat conduction through the bubble wall is no longer independent of the radial position of the laser spot. A thermal resistance can, however, be defined as follows:

$$R_{th} = (T_1 - T_2)/Q = (T(r_1) - T_2)/Q, \quad (35)$$

where $T(r_1)$ is calculated using Eqs. (30), (33), and (34), and after substitution

$$R_{th} = (T_{env} - T_1)/Q + i[Y_0(-i\beta r_2)J_0(i\beta r_1) - J_0(i\beta r_2)Y_0(-i\beta r_1)]/D.$$

The calculated temperature as a function of heat transfer coefficient h at the graphene surface is shown in Fig. 5. To reach a temperature at the center of the bubble of 1050 to 1200 °C according to experimental results, see Fig. 3, the heat transfer coefficient h must be in the range of 20 000 to 40 000 W m^{-2}K^{-1}. Assuming the gas in the bubble is air with a thermal conductivity of 0.02 W m^{-1}K^{-1}, this heat transfer coefficient corresponds to an equivalent conductive layer varying from 1 to 0.5 μm which is compatible with the height of the bubble shown in Fig. 2. This shows that the heat transfer rate through the gas inside the bubble is not negligible and needs to be taken into account. It represents 53% and up to 74% when h varies from 20 000 to 40 000 W m^{-2} K^{-1}.

C. Asymmetric heat conduction including gas inside bubble

When the laser spot is off center, the temperature field is three dimensional for the gas inside the bubble. No analytical solution of the heat equation can be found and temperature distribution can be obtained by numerical finite volume calculations. The finite volume method takes into account a spherical cap and the bubble wall. Figures 6 and 7 show the mesh structure used for the numerical calculations. The mesh density is larger at the boundaries to account for the large contrast of the thermal conductivity in the bubble wall and the gas inside the bubble.

The heat transfer above the graphene bubble is neglected and it is assumed that the silicon substrate remains at room temperature; the edge of the bubble is maintained at room temperature. The laser spot is modeled by a constant heat flow rate imposed on a disk of radius 0.5 μm that is located at variable

radial position. Symmetry allows to reduce the calculation to half of the bubble. The calculations are carried out using a commercial software (STAR-CCM+, Siemens) which allows to solve the heat equation in the graphene layer using the thin layer coupled with a full three-dimensional gas volume. The heat flow in the bubble wall was considered two dimensional (shell) while in the gas inside the bubble the heat flow was considered three dimensional (see Siemens Simcenter STAR-CCM + software for details).

The gas volume is small and narrow, particularly near the bubble border where the section in the radial direction is triangular. After testing mesh convergence, a highly refined mesh was chosen (10 619 242 polyhedral cells in the air and 3 119 582 shell cells in the graphene, see Figs. 6 and 7 to model correctly the high contrast of thermal conductivity ($k_g/k_f \approx 50\,000$). The numerical solution is reliable since (i) the residual is low and stable; (ii) the local and individual heat balances is observed (less than 0.1% error). The numerical calculation was also applied to the symmetric case described in Sec. III A to test the numerical calculations. Excellent agreement was obtained. The temperature of the
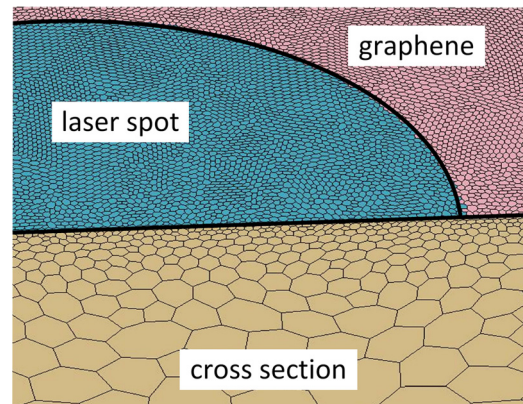

FIG. 7. Detailed view of mesh used in the numerical calculation at the edge between laser spot, bubble wall, and vertical plane across bubble. Mesh density increases near the border to accommodate large contrast in thermal conductivity.
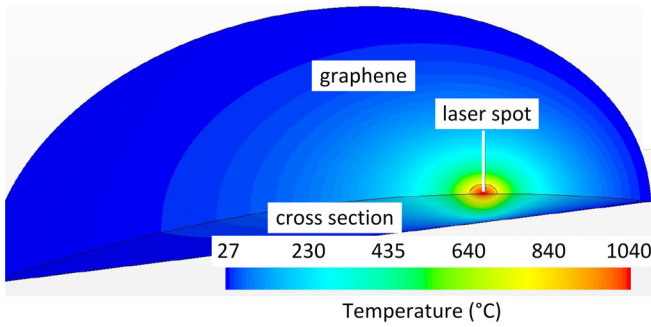
FIG. 8. View from top of bubble and temperature field in graphene and in gas inside bubble along symmetry plane for laser spot centered at half radius, substrate temperature was $27\,^{\circ}$C.

silicon substrate was verified to stay within 5 K of 300 K during preliminary calculations and 300 K in the results presented here.

The calculations were first carried out considering constant thermal conductivity and heat capacity and then compared to when including the temperature dependence of the heat conductivity. A significant influence was observed due to the temperature variation of the thermal conductivity. The thermal conductivity of the fluid varies by one order of magnitude in the considered temperature range (0.025 W m^{-1} K^{-1} at 300 K and 0.2 W m^{-1} K^{-1} at 1300 K).

The laser spot was first placed at the center of the bubble and the calculated temperature profile in the graphene, the heat flow rate distribution within the graphene and the trapped gas is stored. The laser spot was then placed on various off center positions and the calculation repeated. For each position of the laser spot the heat flow rate has been varied according to the possible limiting values of the reflectance of the substrate ($0 < \Gamma < 1$).

It is noted since the results described below are expressed in terms of heat flow rate, they can also be used if the laser power or the graphene absorbtion differs from the values used here.

An example of the temperature field obtained is shown shown in Fig. 8 in the case the laser spot being located at $x_{C2} - x_{C1} = r_2/2$. The maximum temperature rises up to more than $1000\,^{\circ}$C at the center of the laser spot and sharply decreases in the radial direction. It is observed that in the region where the heat flow rate is fixed the temperature varies strongly, although the diameter of this zone is small: in Fig. 8 the temperature at the center of the laser spot is about $1040\,^{\circ}$C while the average temperature is $940\,^{\circ}$C.

The maximum and mean temperatures of the spot region are then determined for various laser spot locations and are compared to the experimental results in Fig. 3. A good agreement with the experimental results is obtained and the maximum calculated temperature remains in between the maxima and minima of the Raman oscillations for all laser spot positions.

D. Discussion of the volume element analysis

The heat flow from the laser spot to the substrate can be described as the superposition of the heat flow from the spot
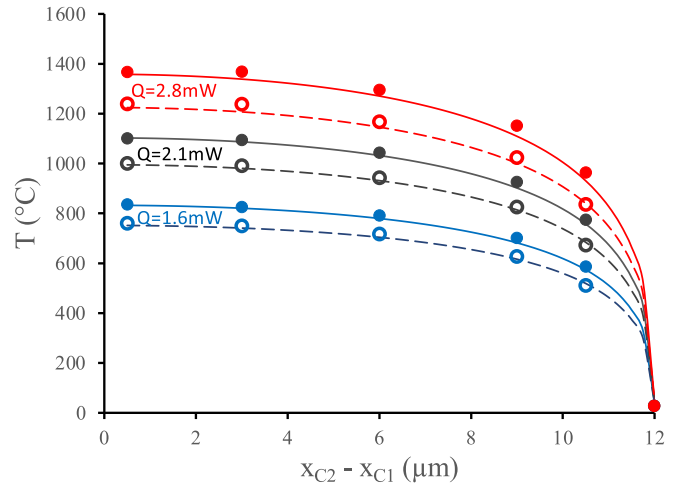

FIG. 9. Maximum and average spot temperature as function of distance between center of the graphene and center of laser spot: comparison of numerical results (symbols) with Eqs. (36) to (38) (lines). Average temperature: empty symbols and dashed lines; maximum temperature: plain symbols and plain lines.

to the substrate through graphene alone and a series of radial heat flows through graphene. The ratio of these two main contributions depends predominantly on the spot location.

It is important to note that the temperature reached in graphene at the laser spot ($1040\,^{\circ}$C) when including heat conduction though the air inside the bubble is significantly lower than when considering only heat conduction through graphene ($2100\,^{\circ}$C).

The results of the finite volume analysis was to confirm a semi-empirical correlation of the temperature of the laser spot versus its position which is independent of the laser power, the absortivity of graphene, and the reflectance of the substrate. To derive this correlation we compare the bubble graphene thermal resistance (i.e., thermal resistance of {graphene-trapped gas}) with the thermal resistance R_{th} of the graphene alone which is given by

$$R_{\text{th}}(\ell) = \frac{1}{2\pi k z}\text{arcosh}\left(\frac{r_1^2 + r_2^2 - \ell^2}{2r_1 r_2}\right). \tag{36}$$

The bubble thermal resistance is derived from the numerical temperature field by either $(T_{\text{max}} - T_2)/Q$ or $(T_{\text{mean}} - T_2)/Q$ depending upon the temperature under consideration. The correlation so obtained is given by

$$T(\ell) = T_{\text{env}} + Q\left(\Omega - \frac{T(\ell = 0)}{1000}\right)[R_{\text{th}}(\ell)]^{\frac{4}{5}}, \tag{37}$$

with

$$T(\ell = 0) = \frac{T_{\text{env}} + \Omega Q[R_{\text{th}}(\ell = 0)]^{\frac{4}{5}}}{1 + \frac{Q}{1000}[R_{\text{th}}(\ell = 0)]^{\frac{4}{5}}}. \tag{38}$$

The value of Ω depends upon the temperature in the laser spot, and either the maximum ($\Omega = 12$) or the mean value ($\Omega = 10.8$) is adopted.

Both maximum and mean spot temperatures calculated with Eqs. (36), (37), and (38) are compared to the numerical results in Fig. 9 for three different heat flow rates, good

overall agreement is observed between numerical and analytical calculations.

IV. ELASTIC PROPERTIES

In was shown that large graphene bubbles can be described by an elastic membrane [13]. This is justified by the small height compared to its diameter. The bubble has, in this case, a kink at the edge and the deflection of the membrane into a bubble implies radial and circumferential strain components. The strain at the edge is uniaxial and at the center it is equibiaxial [13]. At equilibrium the total energy is minimized which yields expressions for the pressure difference and the adhesion energy. The adhesion energy and pressure difference can then be expressed as a function of the ratio of the bubble height and the radius of the bubble, the elastic modulus of graphene and its Poisson's ratio [13]. Recently it was reported [14] that the shape of the bubble which can be described by a function of the ratio of the bubble height to radius with an exponent q: that varies between 2 and 2.3 depending on the ratio of height to radius. Taking the height and radius of the bubble in Fig. 2 $q = 2.15$ [14]. The adhesion energy is given by

$$\Gamma = \frac{5}{8\phi} E \left(\frac{h}{a} \right)^4, \qquad (39)$$

where E is the elastic modulus of graphene, h the bubble height, a the bubble radius, and ϕ is a function of the Poisson's ratio ν,

$$\phi = \frac{75(1 - \nu^2)}{8(23 + 18\nu - 3\nu^2)}, \qquad (40)$$

and $\nu = 0.16$ [13].

Assuming that the same relations apply to the swelling, the elastic modulus of graphene in the swelling region can be deduced by the ratio of the height to radius

$$E_s = E_b \cdot \left(\frac{h_b a_s}{h_s a_b} \right)^4. \qquad (41)$$

Using for the diameter and height of the swelling and the bubble a_s, a_b and h_s, h_b, 3.6, 12.7 and 0.6, 1.0 yields $E_s = 0.57 \cdot E_b$. This means the elastic modulus above 1000 °C is reduced by at least 43% of its value at room temperature. However, the dependence on the fourth power makes the result depend strongly on the errors in the measurement of the h and a. Assuming a relative error in the measurement of the radius and height of of 3% results in overall error of 24%. The value given here represents a lower limit of the reduction of the elastic modulus at 1000 °C.

Alternatively, the reduction of the Young's modulus can be estimated by the temperature dependence of bending rigidity of graphene using molecular dynamics simulations [15]. Bending rigidity in graphene is reduced from 0.88 eV to 0.46 eV when increasing the temperature from room temperature to 1000 °C [15], a reduction of 52%. The graphene we consider is a bilayer graphene. Bending rigidity for a plate is proportional to the third power of the elastic thickness, but drastically reduced in few-layer graphene. Bending stress is relieved through shear and slip rather than in-plane stress. For bilayer graphene the bending rigidity is double the value for single-layer graphene [16]. The reduction of the bending rigidity with temperature is assumed the same and accordingly the same reduction of the Young's modulus with temperature is assumed. Since the bending rigidity is proportional to the Young's modulus for membranes this means that the Young's modulus is reduced by the same amount, which is reasonably consistent with reduction of 43% in the Young's modulus described above.

V. CONCLUSION

Laser heating of "large" graphene bubbles enabled heating graphene bubbles above 1000 °C. Reduction of the Young's modulus and bending rigidity at elevated temperature leads to the appearance of a swelling on the bubble. The swelling geometry is deduced from Raman G band oscillations which measure the distance of the graphene with respect to the substrate under laser excitation. When taking into account heat transport through graphene only, analytical expressions for the temperature are derived. The so-determined temperature exceeds 2000 °C at the center of the bubble. When including heat conduction through the gas inside the bubble employing finite volume analysis, it is found that heat conduction through the gas in the bubble is significant and lowers the maximum temperature at the center of the bubble to below 1400 °C. Semi-empirical expressions were deduced for the temperature distribution as a function of the position of the laser spot. The appearance of a swelling in large graphene bubbles when laser heated might eventually find application for creating a central hole in graphene membranes.

ACKNOWLEDGMENTS

[1] D. G. Papageorgiou, I. A. Kinloch, and R. J. Young, Prog. Mater. Sci. **90**, 75 (2017).

[2] T. Shao, B. Wen, R. Melnik, Y. K. S. Yao, and Y. Tian, J. Chem. Phys. **137**, 194901 (2012).

[3] K. Kim, W. Regan, B. Geng, B. Alemán, B. M. Kessler, F. Wang, M. F. Crommie, and A. Zettl, Phys. Status Solidi (RRL) **4**, 302 (2010).

[4] S. Deng and V. Berry, Mater. Today **19**, 197 (2016).

[5] Y. Huang, X. Wang, X. Zhang, X. Chen, B. Li, B. Wang, M. Huang, C. Zhu, X. Zhang, W. S. Bacsa, F. Ding, and R. S. Ruoff, Phys. Rev. Lett. **120**, 186104 (2018).

[6] P. L. de Andres, F. Guinea, and M. I. Katsnelson, Phys. Rev. B **86**, 144103 (2012).

[7] V. V. E. Pop and A. Roy, MRS Bull. **37**, 1273 (2012).

[8] W. Bacsa, R. Bacsa, and T. Myers, *Optics Near Surfaces and at the Nanometer Scale* (Springer, Cham, Germany, 2020), Chapter Springer Briefs in Physics.

[9] M. Bruna, A. K. Ott, M. Ijäs, D. Yoon, U. Sassi, and A. C. Ferrari, ACS Nano **8**, 7432 (2014).

[10] J. Zabel, R. R. Nair, A. Ott, T. Geargiou, A. K. Geim, K. S. Novoselov, and C. Casiraghi, Nano Lett. **12**, 617 (2012).

[11] I. Calizo, S. Ghosh, A. Bao, C. Lau, and A. Balandin, Solid State Commun. **149**, 1132 (2009).

[12] H. Carslaw and J. Jaeger, *Conduction of Heat in Solids*, 2nd ed., (Oxford at Clarendon Press, New York, 1959).

[13] K. Yue, W. Gao, R. Huang, and K. Liechti, J. Appl. Phys. **112**, 083512 (2012).

[14] E. Blundo, T. Yildirim, G. Pettinari, and A. Polimeni, Phys. Rev. Lett. **127**, 046101 (2021).

[15] P. Liu and Y. Zhang, Appl. Phys. Lett. **94**, 231912 (2009).

[16] E. Han, J. Yu, E. Annevelink, J. Son, D. Kang, K. Watanabe, T. Taniguchi, E. Ertekin, P. Y. Huang, and A. derZande, Nat. Mater. **19**, 305 (2020).